Journal of Electroanalytical Chemistry 765 (2016) 8–15

Contents lists available at ScienceDirect

Journal of Electroanalytical Chemistry

journal homepage: www.elsevier.com/locate/jelechem

Development and characterization of carbon based electrodes from pyrolyzed paper for biosensing applications

Jason G. Giuliani [a], Tomás E. Benavidez [b], Gema M. Duran [c], Ekaterina Vinogradova [d], Angel Rios [c], Carlos D. Garcia [b,*]

[a] Department of Chemistry, The University of Texas at San Antonio, San Antonio, TX 78249, USA
[b] Department of Chemistry, Clemson University, Clemson, SC 29634, USA
[c] Department of Analytical Chemistry and Food Technology, University of Castilla–La Mancha, Ciudad Real, Spain
[d] Department of Physics and Astronomy, The University of Texas at San Antonio, San Antonio, TX 78249, USA

ARTICLE INFO

Article history:
Received 31 March 2015
Received in revised form 3 July 2015
Accepted 31 July 2015
Available online 16 August 2015

Keywords:
Carbon
Pyrolysis
Biosensor
Uric acid
Paper

ABSTRACT

This article details the study of electrochemical behavior of new carbon electrodes based on pyrolysis of different paper sources to be used in biosensor applications. The resistivity of the pyrolyzed papers was initially used as screening parameters to select the best three paper samples (imaging card paper, multipurpose printing paper, and 3MM chromatography paper) and assemble working electrodes that were further characterized by a combination of microscopy, electrochemistry, and spectroscopy. Although slight differences in performance were observed, all carbon substrates fabricated from pyrolysis of paper allowed the development of competitive biosensors for uric acid. The presented results demonstrate the potential of these electrodes for sensing applications and highlight the potential advantages of 3MM chromatography paper as a substrate to fabricate electrodes by pyrolysis.

© 2015 Elsevier B.V. All rights reserved.

1. Introduction

Since the first report in 1962 [1], the field of biosensors has made astounding progress. Doctors and patients are increasingly relying on simple, fast, and cost-effective biosensors to monitor a variety of analytes [2]. Although a variety of biosensors are currently available, the versatility of electrochemical biosensors clearly stands out in the move towards simplified testing [3]. Electrochemical biosensors have now moved beyond the classic examples involving glucose oxidase and have been adapted to quantify a wide range of analytes, feature adequate sensitivity for clinical applications, offer independence from optical interferences, require minimal sample and power consumption, and are highly compatible with modern microfabrication techniques [4–7]. Moreover, coupling the simplicity of the instrumental requirements of electrochemical detectors with the increased availability and computing capabilities of mobile phones, several groups have developed portable electrochemical platforms that could soon be adapted to biosensing applications [8–10]. It is also clear that along with the growth in the use of these devices, demands for cost and time-effective ways to produce biosensors are also increasing. In this regard, one of the most important points to consider is the selection of the transducer. While recent advances in nanotechnology have allowed the development of improved sensors based on modified metallic surfaces, the vast majority of the community has opted for carbon-based material [11–13]. Aside from traditional examples such as glassy carbon [14] and mesoporous carbon [15], carbon-based nanomaterials (nanodiamonds, nanofibers, nanorings, and nanotubes) [16,17] share a common structure composed of sp^2-bonded atoms that supports electrical conductivity [16], the capacity to form charge-transfer complexes [18], unique optical properties [19], chemical reactivity [20,21], and the possibility to interact with a variety of biorecognition elements [22].

Because most of these materials also share the high costs and limited accessibility linked to the fabrication methods (such as chemical vapor deposition or screen-printed electrodes) [23–25], many researchers have focused their attention on the development of platforms that are more suitable for the needs in low-income communities. Among them, it is important to highlight the possibility to fabricate electrodes from carbon-ink or pyrolysis of organic precursors. The former electrodes have been micromolded using PDMS [26], painted over Au wires [27], and more recently adapted to perform detection in paper-based microfluidic devices [28,29]. The latter electrodes can be fabricated by pyrolysis from a variety of organic precursors including photoresist [30–35], parylene C [36], proteins [37] or even insects [38]. While all these materials have the potential to enable operational electrochemical sensors, most of them offer limited surface area and their application for

* Corresponding author at: 219 Hunter Laboratories, Clemson, SC 29634, USA.
E-mail address: cdgarci@clemson.edu (C.D. Garcia).

http://dx.doi.org/10.1016/j.jelechem.2015.07.055
1572-6657/© 2015 Elsevier B.V. All rights reserved.

the development of electrochemical biosensors is restricted by the resistivity of the material, which results in quasi-reversible [39,40] or irreversible electrochemical behavior [37,41].

To address these deficiencies, this report describes the possibility to prepare electrodes by pyrolysis of paper. The resulting electrodes, which can be fabricated from a variety of substrates, feature low resistivity, large surface area, and uniform thickness. More importantly, the electrodes can be used for the development of biosensors by simply immersing them in a solution containing a selected enzyme. Herein we present results related to the selection of the substrate, the characterization performed (microscopy and electrochemical) as well as their potential for the development of an electrochemical biosensor for uric acid.

2. Materials and methods

2.1. Reagents

Recombinant uricase (also known as urate oxidase) from *Candida* sp. expressed in *Escherichia coli* and potassium hexacyanoferrate (III) were purchased from Sigma-Aldrich (St. Louis, MO, USA). Uric acid, 99% was obtained from Alfa Aesar (Ward Hill, MA, USA). Sulfuric acid (ACS/FCC, BDH ARISTAR, 95.0–98.0%) was acquired from VWR (Pittsburgh, PA, USA). All aqueous solutions were prepared using 18 MΩ·cm water (NANOpure Diamond, Barnstead; Dubuque, IA) and analytical reagent grade chemicals. Phosphate buffer solution was prepared by dissolving anhydrous Na_2HPO_4 (Fisher Scientific; Fair Lawn, NJ, USA) in ultrapure water. The pH of the solutions was measured using a glass electrode connected to a digital pH meter (Orion 420A+, Thermo; Waltham, MA, USA) and adjusted with 1 $mol \cdot L^{-1}$ solutions of either NaOH or HCl. Standard uric acid solution was freshly prepared in phosphate buffer solution (10 $mmol \cdot L^{-1}$, pH = 8.5) before each experiment.

2.2. Carbon electrode fabrication

Electrodes described in this manuscript were fabricated by pyrolysis of commercially available paper samples and used as received. In order to probe a range of potential substrates, multipurpose printing paper (75 $g \cdot m^{-2}$, Spectrum; El Paso, TX), JP40 filter paper (80 $g \cdot m^{-2}$, Quanty; J-Prolab, Brazil), Gilbert 100% Cotton Linen Paper (90 $g \cdot m^{-2}$, Neenah Paper; Neenah, WI), Whatman filter paper #4 (96 $g \cdot m^{-2}$, GE Healthcare; Pittsburgh, PA), drawing paper (130 $g \cdot m^{-2}$, Strathmore; Appleton, WI), imaging card paper (138 $g \cdot m^{-2}$; JetPrint; Memphis, TN), Whatman 3MM Chromatography Paper (189 $g \cdot m^{-2}$, GE Healthcare; Pittsburgh, PA), and Wausau Astroparche (220 $g \cdot m^{-2}$, Neenah Paper; Neenah, WI) were selected. The selection was made based on availability and not by the composition of the paper, which is proprietary information.

The electrodes were fabricated using a procedure adapted from a previous publication from our group [37,41]. Briefly, 2.5 cm × 5 cm pieces of paper were cut and placed in a tube furnace (Type F21100, Barnstead–Thermolyne; Dubuque, IA, USA). The tube furnace was then flushed for 5 min with Ar (to remove the O_2 from the quartz tube and avoid oxidation reactions) and turned on. Once the furnace reached 1000 °C (typically within 30 min, see Supplementary Information), 5% H_2 was added to the Ar flow to create a reducing environment and flowed in the tube for 1 h. Next, the hydrogen was turned off and the tube furnace was allowed to cool down to room temperature under 100% Ar flow (typically about 1 h). The samples were then removed from the furnace and affixed to a Plexiglas substrate using double sided tape. In order to define a uniform electrode size, the electrodes were then patterned using a commercial CO_2 laser engraver (Mini24, Epilog Laser Systems; Golden, CO, USA) [42–44], defining electrodes like the one shown in Fig. 1. To keep water from wicking up the stem of the electrode (and modifying the electrode area), paraffin paper was wrapped around the base of the stem (between the circular pad and the contact area) and melted in place using a hot air gun. Finally, silver paint (SPI Supplies; West Chester, PA, USA) was applied to the tip of the stem to define a contact area for the potentiostat. The resistance of the electrical contact (<60 mΩ/sq./mil) was considered negligible with respect to that of the carbon electrode.

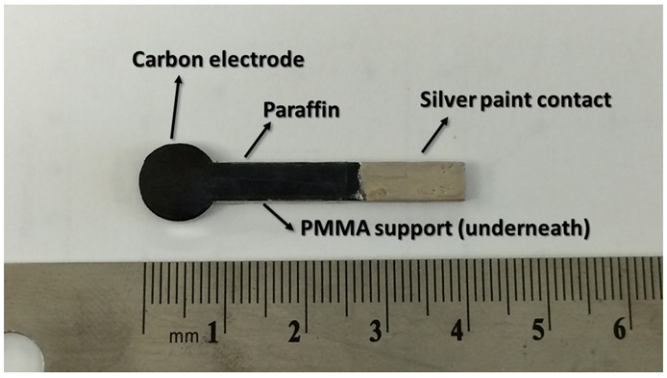

Fig. 1. Photography of one electrode fabricated using pyrolyzed paper. Figure also shows the section coated with paraffin and the section coated with silver paint.

2.3. Electrochemical techniques

Cyclic voltammetry (CV) and electrochemical impedance spectroscopy (EIS) were employed to investigate the electrochemical performance of the carbon electrodes produced from paper. The experiments were performed using 100 $mmol \cdot L^{-1}$ H_2SO_4, as supporting electrolyte, containing 1.0 $mmol \cdot L^{-1}$ $Fe(CN)_6^{3-}/Fe(CN)_6^{4-}$, as the redox couple. In all cases, a standard three-electrode cell comprised of the paper-derived electrodes, a silver/silver chloride ($Ag|AgCl|KCl_{sat}$), and a platinum wire were used as working, reference, and counter electrode, respectively. CV experiments were carried out using a CHI812 Electrochemical Analyzer (CH Instruments, Inc.; Austin, TX). EIS data were obtained using a PC-controlled CHI 660A potentiostat by scanning from 10^{-4} Hz to 10^5 Hz at a 5 mV amplitude, with 10 data points per frequency decade. The impedance spectra were then analyzed with the simulation software *Zview*-Impedance® (version 2.4a) by fitting the spectra with a Randles-type equivalent circuit.

2.4. Thermogravimetric analysis

The pyrolysis of the paper samples was studied by measuring the weight loss of the selected samples while the temperature was increased at 5 °C·min^{-1} from 21 °C to 800 °C using a TGA-50 Thermogravimetric Analyzer (Shimadzu Corp.; Tokyo, Japan). TGA experiments were performed in the presence of pure N_2 as an inert purge gas to prevent undesirable reactions between the paper samples and air. The N_2 was also used to remove the gaseous and condensable products evolved during the paper pyrolysis. As a negative control, silica nanopowder was used.

2.5. Raman spectroscopy

A confocal Raman automated imaging spectrometer (iHR320, Horiba Jobin Yvon) was used to examine the composition of the carbon electrodes from pyrolyzed paper. The Raman spectrometer was equipped with an excitation laser of 488 nm wavelength and a Synapse CCD detector. The Raman spectra were collected in the 1000–1800 cm^{-1} range, with an exposure time of 2 s, an accumulation factor of 2, and with a 100× objective.

2.6. Uric acid biosensor

To obtain an amperometric biosensor for uric acid, the selected carbon electrodes were immersed in a phosphate buffer solution

($10\ mmol \cdot L^{-1}$, pH = 5.4) containing $1\ mg \cdot mL^{-1}$ uricase for 1 h under gentle agitation (80 rpm using a platform shaker, Innova 2000, New Brunswick Scientific; Edison, NJ, USA). This procedure allows the spontaneous adsorption of the enzyme on the electrode surface [22]. Although this solution has limited buffer capacity ($\beta = 3.6 \times 10^{-4}$), the pH value was selected to match the isoelectric point of the protein and therefore minimize inter-protein electrostatic repulsions and maximize the amount of enzyme adsorbed. After the enzyme immobilization, each electrode was gently rinsed with buffer solution (to remove the enzyme molecules loosely bound to the electrode surface) and transferred to the electrochemical cell containing 35 mL of $10\ mmol \cdot L^{-1}$ phosphate buffer at pH = 8.5 (the optimum pH of the enzyme). In order to evaluate the performance of the biosensor, calibration curves were carried out by adding known amounts of uric acid and following the H_2O_2 released according to the following reaction:

$$\text{Uric acid} + O_2 \xrightarrow{\text{uricase}} \text{Allantoin} + CO_2 + H_2O_2. \quad (1)$$

As a compromise between signal magnitude and selectivity [45,46], the oxidation of hydrogen peroxide was performed at +650 mV (vs. $Ag|AgCl|KCl_{sat}$) and followed by chronoamperometry.

2.7. Safety considerations

Sulfuric acid can cause burns and death if not handled with care. The tube furnace operates at temperatures of up to 1200 °C and contains a mixture of 95% Argon and 5% Hydrogen. Because hydrogen gas is extremely flammable, the described procedure requires great care and vigilance.

3. Results and discussion

3.1. Resistivity, shrinkage, and strength of carbonized papers

In order to gain preliminary information related to the macroscopic properties of the carbonized papers, the resistance (Ω) was measured using a standard digital multimeter (2216-20 TRMS multimeter, Milwaukee Electric Tool Corp.; Brookfield, WI). In all cases, samples of 1 cm × 3 cm were used. To improve the electrical contact with the multimeter connectors, silver paint was applied to the edges of the pyrolyzed paper samples. The obtained values were used to calculate the corresponding resistivity (ρ), as expressed by the Eq. (2),

$$\rho = {}^{\Omega A}/_{l} \quad (2)$$

where A is the cross-sectional area and l the distance between the measuring electrodes. Because the resistivity is an intrinsic property of materials, resistance values measured at varying distances were used to evaluate the uniformity of the produced electrodes. Fig. 2A summarizes the results obtained for the resistivity of the electrodes as a function of the initial paper basis weight.

As it can be observed, all selected papers yielded electrodes with resistivity values lower than 1 Ω·cm, which were considered significantly better than other stand-alone carbon-based materials used in electrochemical detectors [37,41,47]. It is also important to point out that no correlation between the basis weight of the paper and the final resistivity of the carbon electrodes was observed. Although these experimental results somehow contradict the initial assumption that heavier paper substrates would contain higher amounts of cellulose and lead to electrodes with lower resistivity values, the differences in resistivity could be attributed to differences in the composition of the papers.

While not related to their electrical properties, it was also observed that the pyrolysis process induced significant decreases in the paper volume (shrinkage). Fig. 2B summarizes the volume loss of the carbon sample after pyrolysis at 1000 °C, as calculated by measuring the length,

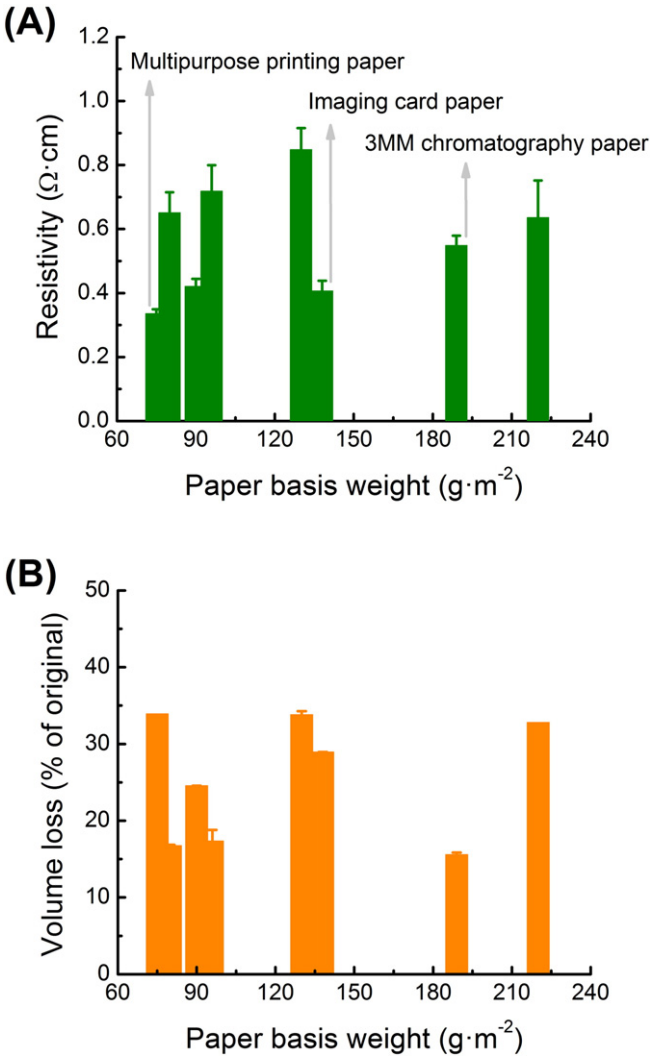

Fig. 2. Resistivity (A) and percentage of volume loss (B) as a function of the paper basis weight before pyrolysis.

width, and thickness using a digital caliper (Neiko tools 01407A). In general, it can be observed that the final dimensions of the carbon electrodes decreased an average of 75 ± 8% with respect to the original values. These results highlight the importance of patterning the electrodes after the pyrolysis. Another significant feature considered in this project was the malleability of the pyrolyzed samples to fabricate carbon electrodes. Although only empirical data was collected (data not shown), pyrolysis of cotton paper yielded rather brittle substrates that easily cracked during handling. Considering the resistance and the fragility of the produced electrodes, the imaging card paper, 3MM chromatography paper, and multipurpose printing paper were selected to assemble working electrodes and used for the remaining experiments described in this article.

3.2. Thermogravimetric analysis

To gain insights into the thermal decomposition process of the selected papers, TGA experiments were performed in the 21 °C to 800 °C range (under N_2) at a heating rate of $5\ °C \cdot min^{-1}$. Representative thermogravimetric curves are shown in Fig. 3.

As it can be observed, a slight weigh loss in the samples (~5%) was always observed from the beginning of the experiments until the temperature reached a value of approximately 115 °C. This process was attributed to the loss of chemical compounds (such as water)

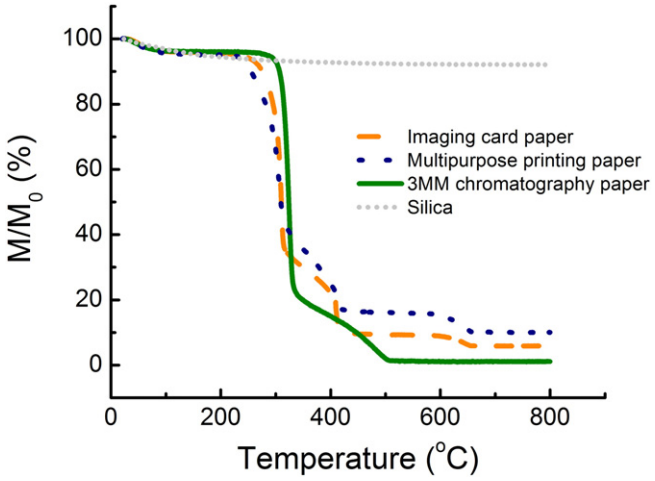

Fig. 3. Thermogravimetric curves obtained for the pyrolysis of imaging card paper, multipurpose printing paper, and 3MM chromatography paper. Silica was used as a control.

weakly bound to the paper. In agreement with previous reports [48–50], the most significant decomposition step was observed in the 216–336 °C range, with a maximum mass loss obtained around 313 °C. This transition stage has been attributed to the breakdown of cellulose through the formation of levoglucosan and other volatile compounds. Unlike pure cellulose that yields a single degradation step [51], one or two more degradation processes were observed at temperatures above 336 °C, in all paper samples. In agreement with previous reports [52, 53], these endothermic processes were attributed to the decomposition of non-cellulosic impurities present in the sample (binders, fillers, inks, etc.). Such components could be responsible for the residues observed in the SEM images (Fig. 4) and the additional redox peaks observed in the voltammograms ($E_{PA} = 248$ mV/$E_{PC} = 154$ mV) obtained with the imaging card paper (Fig. 6A). Considering these results, a pyrolysis temperature of 1000 °C was selected for the fabrication of electrodes from different paper sources. Although the selected value is in line with the pyrolysis temperatures selected for the production of other carbon electrodes [37,41,54] the presented TGA results suggest that lower temperatures (~600 °C) could be sufficient for the fabrication of electrodes from pyrolyzed 3MM chromatography paper (>98% cellulose).

3.3. Surface topography

Scanning electron micrographs were obtained to evaluate surface topography of the electrodes produced by pyrolysis of the selected papers. Fig. 4 shows representative examples of the structures obtained with each of the selected papers. The image also shows that the fiber structure of the cellulose [42,43] was preserved in all cases, resulting in a mesh of highly porous carbonized material with fibers of 8 ± 2 μm (n = 25) in diameter. As it can be also observed in the SEM micrographs, a significant amount of amorphous material was also observed in the carbon electrodes fabricated by pyrolysis of imaging card paper (Fig. 4A) and, to a larger extent, multipurpose printing paper (Fig. 4B). These results are in agreement with the results obtained by TGA and cyclic voltammetry (vide infra) and suggest that the additives found in the imaging card paper and multipurpose paper yielded to the formation of this material that remained (~10% of the initial weight of the paper sample, see Fig. 3) after the pyrolysis.

3.4. Microstructure of the substrates

It is known that carbon has several allotropes and that each form has a different contribution to the electronic properties of the material [55]. For this reason, Raman spectroscopy was used to obtain structural

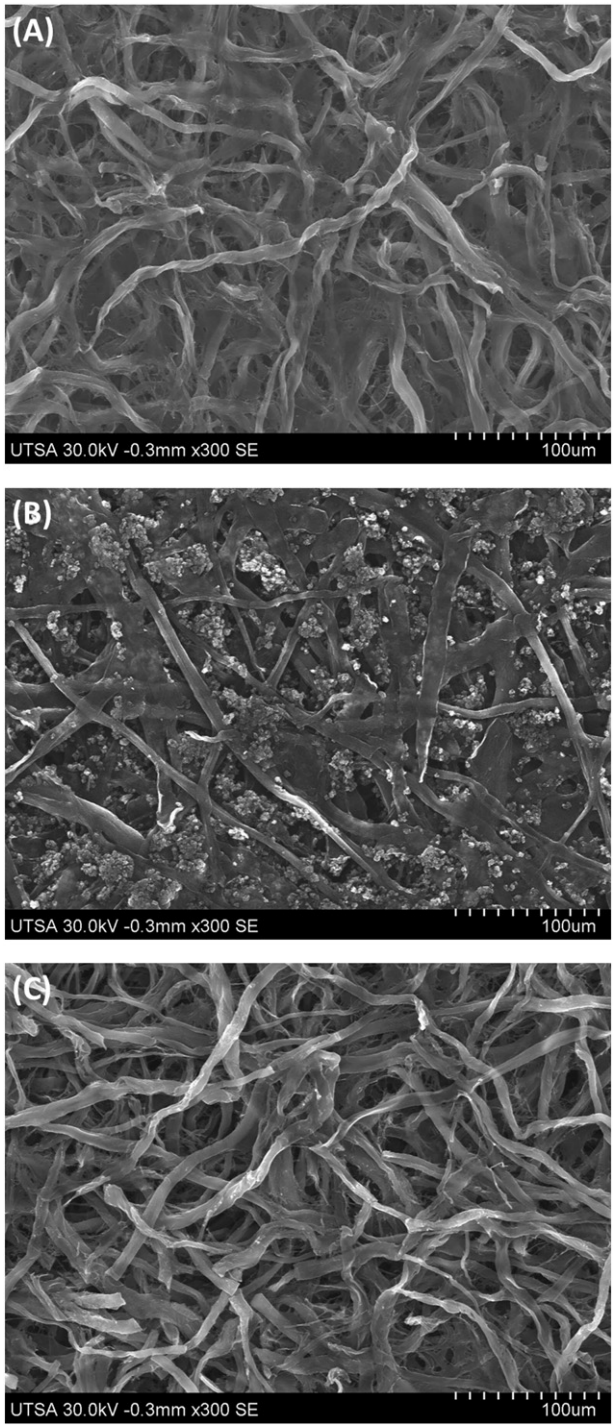

Fig. 4. SEM micrographs of the working carbon electrodes obtained from pyrolysis of imaging card paper (A), multipurpose printing paper (B), and 3MM chromatography paper (C).

information related to the carbon electrodes produced from different papers substrates. The results were then analyzed to calculate the relative intensity of the G band and the D band, which have been attributed to the breathing of C–C bonds in graphite-like carbon (sp^2) and amorphous carbon, respectively. In agreement with previous reports [41,56,57], both bands were observed in the Raman spectra of the substrates produced from the three selected papers (Fig. 5), confirming the presence of both carbon allotropes. It is also important to note that the three selected substrates yielded spectra with similar relative intensities, suggesting that the D/G fraction is not determined by the type of paper selected.

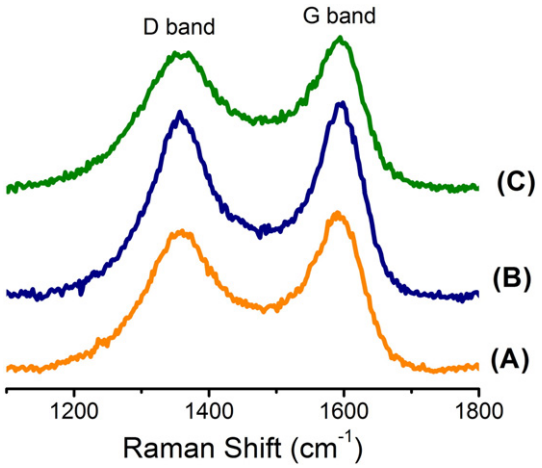

Fig. 5. Raman spectra of the carbon samples obtained by pyrolysis of imaging card paper (A), multipurpose printing paper (B), and 3MM chromatography paper (C).

To analyze the experimental results, Raman spectra were deconvoluted into two Lorentzian peaks centered at 1360 cm^{-1} (D band) and 1590 cm^{-1} (G band). In agreement with previous experiments performed under similar conditions [56], the D/G ratio was found to be 1.5 ± 0.1. This ratio is significantly lower than the one reported for pyrolytic carbon (~4) [36] and suggests the presence of a significant amount of graphitic carbon in the structure of the layer that could support the formation of the π-conjugated system [58]. In line with this observation, the substrates showed relatively low resistivity, a result that highlights the relevance of these materials with respect to electrodes fabricated with thin films [37,41].

3.5. Electrochemical behavior

The electrochemical behavior of the selected carbon electrodes was investigated by cyclic voltammetry using solutions of 100 mmol·L^{-1} H_2SO_4 containing 1.0 mmol·L^{-1} $Fe(CN)_6^{3-}/Fe(CN)_6^{4-}$. This electrochemical couple was chosen because it is a known reversible redox system which is able to provide information about the kinetic performance of the new working electrodes [59]. As it can be observed in Fig. 6, the cyclic voltammograms (performed in the −0.2 V to 1.0 V potential range) showed well-defined redox peaks for the reduction and oxidation of $Fe(CN)_6^{3-}$ and $Fe(CN)_6^{4-}$, respectively. In agreement with the potential values reported to the couple under similar experimental conditions [60], peak potentials in the 308–344 mV and 399–440 mV ranges where obtained for the anodic and cathodic process, respectively. It is also important to note that an additional pair of redox peaks was observed in the electrode produced from imaging card paper. These peaks (that were also present in the blank experiments) were attributed to the presence of residues from additives in the paper to improve its appearance (binders, inks, glossy finish, etc.).

In order to obtain information about the electrochemical process occurring at the electrodes produced from pyrolyzed paper, cyclic voltammograms of $Fe(CN)_6^{3-}/Fe(CN)_6^{4-}$ were recorded at different scan rates, in the 5 mV·s^{-1} to 250 mV·s^{-1} range. For a fully reversible process, the peak current can be described by Eq. (3),

$$ip = 2.69 \times 10^5 n^{3/2} v^{1/2} D^{1/2} AC \quad (3)$$

where n is the number of electrons transferred between the electroactive species in solution and the electrode, v is the scan rate, D is the diffusion coefficient ($cm^{-2}\cdot s^{-1}$), A is the electrode area, and C is the concentration of the electroactive species expressed in mol·L^{-1}. As it can be observed in Fig. 7A, the peak current of both electrochemical processes (reduction and oxidation) increased linearly with the square root of the scan rate in all tested carbon electrodes, suggesting that the electrochemical process in

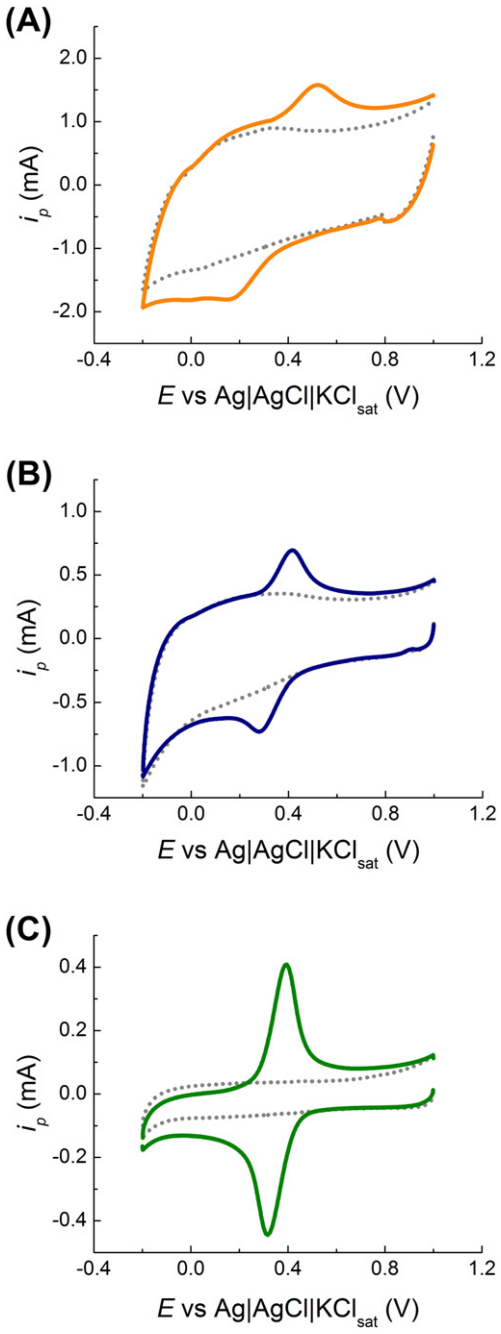

Fig. 6. Cyclic voltammograms of the electrodes fabricated with imaging card paper (A), multipurpose printing paper (B), and 3MM chromatography paper (C). Conditions: 100 mmol·L^{-1} H_2SO_4 containing 1.0 mmol·L^{-1} $Fe(CN)_6^{3-}/Fe(CN)_6^{4-}$, scan rate = 50 mV·$s^{-1}$.

all electrodes was controlled by the diffusion of the analyte from the bulk of the solution to the electrode surface. The ratio of peak heights (i_{pa}/i_{pc}) revealed a slight difference for the carbon electrodes obtained from 3MM chromatography paper (0.97). On the other hand, the carbonized multipurpose printing paper and imaging card paper yielded peak height rations of 0.88 and 0.90, respectively. To identify the roots of these differences (that have been reported for other carbon-based electrodes [29,37,39,40] and evidence a quasi-reversible electrochemical behavior), the ΔEp as a function of the scan rate was also calculated (Fig. 7B).

In contrast with fully-reversible systems that feature peak potential differences ($\Delta Ep = E_{pa} - E_{pc}$) equal to 0.059/$n$ and independent of the scan rate, all electrodes fabricated from pyrolyzed paper yielded a

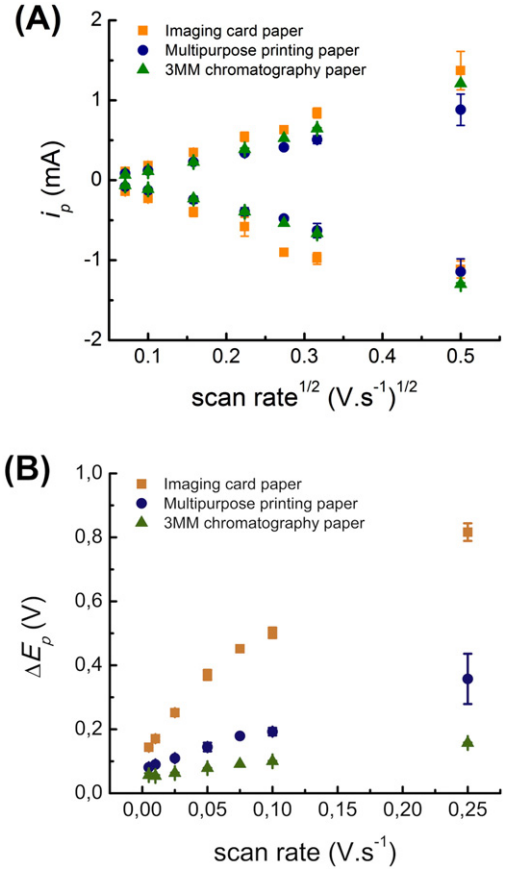

Fig. 7. Dependence of the peak current (i_p) with respect to the square root of the scan rate (A) and dependence of the peak potential difference (ΔEp) with respect to the scan rate (B) for electrodes fabricated by pyrolysis of imaging card paper, multipurpose printing paper, and 3MM chromatography paper.

significant dependence of the ΔEp with respect to the scan rate. These results are characteristic of slow electron transfer kinetics and indicate that the performance of electrodes fabricated from pyrolyzed paper could be limited by the resistance of the resulting material. Moreover, electrodes fabricated from pyrolyzed paper showed significant differences in the background capacitance current (as shown in Fig. 6 and summarized in Table 1). In this regard, it should be noted that electrodes fabricated with 3MM chromatography paper displayed a capacitive current that was almost one order of magnitude lower than those obtained with other paper samples, further supporting their potential to obtain sensors with competitive limits of detection [61].

It is also important to point out that not only the electrochemical reversibility but also the electroactive surface area (ESA) are relevant for the rational selection of substrates as platforms for the development of biosensors. In this regard, cyclic voltammograms of $Fe(CN)_6^{3-}/Fe(CN)_6^{4-}$ recorded at different scan rates (in the 5 mV·s^{-1} to 250 mV·s^{-1} range) were analyzed to calculate the ESA of each electrode from the slope of the Randle–Sevcik plot (Fig. 7A). The ESA is related to the density of electroactive sites on the electrode surface which can transfer the charge between the electrode and the electroactive species in solution. As summarized in Table 1, despite having the relatively poor electrochemical performance, the electrodes fabricated from imaging card paper and multipurpose printing paper displayed large electroactive surface areas (approximately 1.4 times the geometric area ($A_{geo} = 0.785$ cm^2) of the patterned electrodes). This behavior was attributed to an important effect of the surface features of the electrode such as roughness and porosity that increased the contact surface area of the electrode with the solution. Moreover, the electrodes fabricated from 3MM chromatography paper displayed the largest electroactive surface area (approximately 1.6 times the A_{geo} of the patterned electrodes).

Table 1
Electrochemical parameters obtained by cyclic voltammetry of the selected carbon electrodes. i_C corresponds to the average capacitive current obtained at the peak potentials for each electrode and ΔEp corresponds to the peak potential difference, both obtained at 50 mV·s^{-1}. Experimental conditions as described in Fig. 6.

Pyrolyzed paper	i_C (mA)	ΔEp (mV)	i_{pa}/i_{pc}	ESA/A_{geo}
Imaging card	1.0 ± 0.2	370	0.90	1.33
Multipurpose	0.4 ± 0.1	145	0.88	1.35
3MM chromatography	0.05 ± 0.02	79	0.97	1.58

In summary, the experimental results herein described indicate that the selected electrochemical couple displayed a quasi-reversible behavior on all the selected substrates. Such behavior can be attributed to a combination of surface features (functional groups, nanostructures, and surface roughness) and internal resistivity of the resulting carbon material. Among the substrates investigated, electrodes fabricated from 3MM chromatography paper displayed the best electrochemical response and the largest rate constants.

3.6. Electrochemical impedance spectroscopy

In order to obtain quantitative information about the electrical behavior of the electrodes fabricated from pyrolyzed paper, electrochemical impedance spectroscopy (EIS) was carried out in the presence of the selected redox couple ($Fe(CN)_6^{3-}/Fe(CN)_6^{4-}$) and at +600 mV (to ensure limiting-current conditions for all three electrodes, see Fig. 6). The results are summarized in Fig. 8.

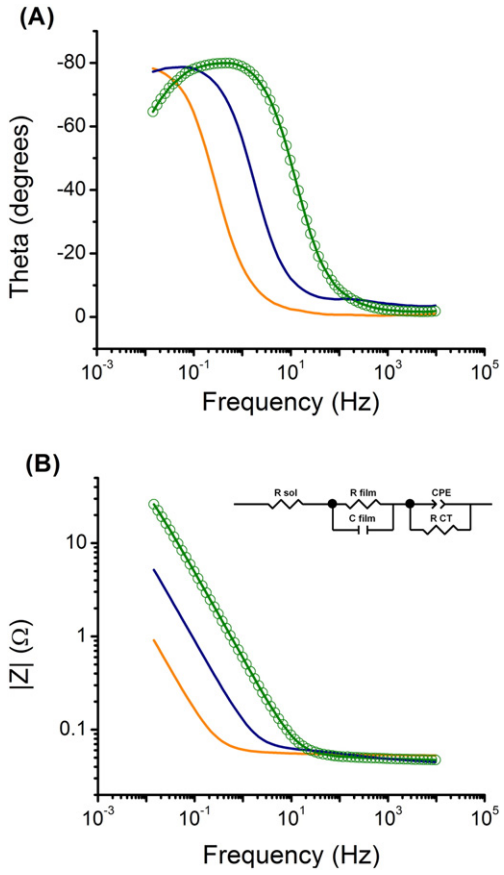

Fig. 8. Dependence of the phase angle (A) and impedance (B) with respect to the frequency for electrodes fabricated by pyrolysis of imaging card paper (orange), multipurpose printing paper (blue), and 3MM chromatography paper (green). Figure also shows the data generated with the equivalent (o) circuit shown as inset in (B).

Fitting the spectra was attempted with several equivalent circuits, but it was not possible to assemble one simple circuit that could describe the electrical properties of all electrodes. This finding was not surprising considering the potential composition, topography (Fig. 4), and limited response (Fig. 6) observed with electrodes fabricated from both imaging card paper and multipurpose printing paper. For the case of electrodes fabricated from 3MM chromatography paper, the obtained spectra was fitted with a Randles-type equivalent electrical circuit (see insert in Fig. 8B), containing elements representing the resistance of the solution ($R_{sol} = 46.6 \pm 0.4\ \Omega$), the internal resistance of the film ($R_{film} = 2.6 \pm 0.1\ \Omega$), the capacitance of the film ($C_{film} = 22 \pm 1\ \mu F$), the charge transfer resistance ($R_{ct} = 63 \pm 2\ k\Omega$), and surface constant phase element (CPE $= 32 \pm 2\ \mu F$) with an exponent constant ($\alpha = 0.93$, instead of the traditional C_{dl} representing the capacitance of the double layer) to account for heterogeneities and roughness of the surface of the electrode [62–64]. These results that are in within the range reported for other carbon electrodes [37,41,65] suggest that the electrochemical process is limited by the R_{ct} rather than the internal resistance of the films.

3.7. Amperometric biosensor

To demonstrate the possible application of carbon electrodes fabricated from pyrolyzed paper, uric acid biosensors were developed by adsorbing uricase onto the substrates [66,67]. After adsorbing the enzyme, each electrode was transferred to the electrochemical cell containing 35 mL phosphate buffer solution (10 mmol L^{-1}, pH = 8.5) and the electrochemical response was recorded by chronoamperometry. Calibration curves were performed by adding known amounts of uric acid dissolved in phosphate buffer (10 mmol L^{-1}, pH = 8.5) and recording the resulting current (oxidation of H_2O_2 at +650 mV). Fig. 9 summarizes the results for calibration curves obtained with electrodes fabricated with imaging card paper, multipurpose printing paper, and 3MM chromatography paper.

As it can be observed, linear relationships between the current and the uric acid concentration were obtained for all electrodes within the range of 0.001 to 0.833 mmol L^{-1}. This linear range is comparable to previously reported values using conventional electrodes [68]. Although the calibration curves were linear up to 0.833 mmol·L^{-1}, the enzyme electrodes showed slight differences in sensitivity. Despite having the poorest electrochemical performance, the biosensor derived from the imaging card paper displayed the highest sensitivity (0.341 ± 0.005 mA·L·$mmol^{-1}$, $R^2 = 0.979$) followed by the one obtained from multipurpose paper (0.237 ± 0.001 mA·L·$mmol^{-1}$, $R^2 = 0.998$), and the electrode obtained from 3MM chromatography paper (0.225 ± 0.002 mA·L·$mmol^{-1}$, $R^2 = 0.995$). These sensitivity values were higher than those reported by Chen [69] and were within the same magnitude than those reported by Chauhan [68]. Additionally, it is important to highlight that the electrode produced from imaging card paper displayed a high dispersion of the experimental data. The limits of detection (LOD) of each electrode were determined based on the standard deviation (s_y) around the trend line obtained by lineal regression and the slope (S) of the calibration curve ($3.3 \times s_y/S$). Although the biosensors developed with the three paper types offered similar analytical performance, the electrode prepared with the 3MM chromatography paper based carbon showed the lowest value (0.004 mmol·L^{-1}), followed by the sensor prepared on multipurpose printing paper (0.006 mmol·L^{-1}) and imaging card paper (0.009 mmol·L^{-1}).

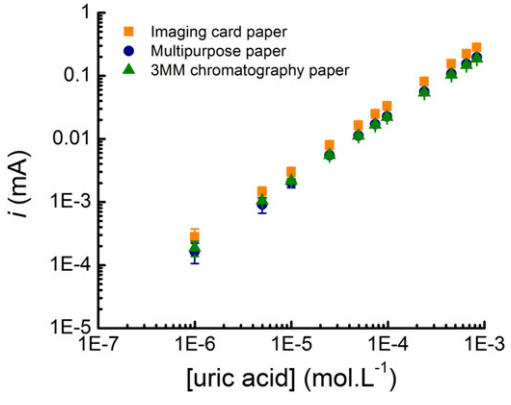

Fig. 9. Calibration curve of enzymatic electrodes obtained by adsorption of uric oxidase onto the selected pyrolyzed paper based carbon electrodes. Error bars represent the standard deviation of experimental data collected with two electrodes fabricated with each paper and repeated at least 4 times.

4. Conclusions

The current article presents the characterization and use of carbon electrodes obtained by pyrolysis of commercially-available paper. Out of the different paper types investigated, imaging card paper, multipurpose printing paper, and 3MM chromatography paper displayed the lowest resistivity and were further characterized. In these cases, the electrodes exhibited a quasi-reversible electrochemical response, controlled by diffusion. In agreement with results obtained by Raman spectroscopy, the electrochemical response was attributed to the large proportion of disordered carbon in the samples, which limits the electron transfer process. Despite these slight differences in performance, the carbon substrates allowed for the successful development of competitive amperometric biosensors for uric acid. Although the presented results demonstrate that standard varieties of commercially available paper can be fashioned into a simple, inexpensive carbon electrodes for sensing applications; electrodes fabricated from 3MM chromatography paper display the best electrochemical response and the lowest resistance.

Acknowledgments

Financial support for this project has been provided in part by NIH Research Centers at Minority Institutions (G12MD007591), NIH National Institute of General Medical Sciences (2SC3GM081085) and the projects CTQ2013-48411-P (MINECO of Spain) and PEIC-2014-001-P (JCCM). J. G. G. thanks the financial support provided by the MBRS-RICE program (GM060655). Gema M. Durán also thanks MINECO of Spain for the predoctoral (BES-2011-045438) and stay (EEBB-I-14-08461) grants. Authors also thank Shane Gerry for initial contributions to this project.

Appendix A. Supplementary data

Supplementary data to this article can be found online at http://dx.doi.org/10.1016/j.jelechem.2015.07.055.

References

[1] L.C. Clark, C. Lyons, Electrode systems for continuous monitoring in cardiovascular surgery, Ann. N. Y. Acad. Sci. 102 (1962) 29–45.
[2] A.P.F. Turner, Biosensors: sense and sensibility, Chem. Soc. Rev. 42 (2013) 3184–3196.
[3] J. Wang, Electrochemical biosensors: towards point-of-care cancer diagnostics, Biosens. Bioelectron. 21 (2006) 1887–1892.
[4] T. Kappes, P.C. Hauser, Electrochemical detection methods in capillary electrophoresis and applications to inorganic species, J. Chromatogr. A 834 (1999) 89–101.
[5] R. Trouillon, M.I. Svensson, E.C. Berglund, A.-S. Cans, A.G. Ewing, Highlights of selected recent electrochemical measurements in living systems, Electrochim. Acta 84 (2012) 84–95.
[6] D.R. Thévenot, K. Toth, R.A. Durst, G.S. Wilson, Electrochemical biosensors: recommended definitions and classification 1, Biosens. Bioelectron. 16 (2001) 121–131.
[7] J. Kirsch, C. Siltanen, Q. Zhou, A. Revzin, A. Simonian, Biosensor technology: recent advances in threat agent detection and medicine, Chem. Soc. Rev. 42 (2013) 8733–8768.
[8] P.B. Lillehoj, M.-C. Huang, N. Truong, C.-M. Ho, Rapid electrochemical detection on a mobile phone, Lab Chip 13 (2013) 2950–2955.
[9] J.L. Delaney, E.H. Doeven, A.J. Harsant, C.F. Hogan, Use of a mobile phone for potentiostatic control with low cost paper-based microfluidic sensors, Anal. Chim. Acta 790 (2013) 56–60.

[10] A. Nemiroski, D.C. Christodouleas, J.W. Hennek, A.A. Kumar, E.J. Maxwell, M.T. Fernández-Abedul, G.M. Whitesides, Universal mobile electrochemical detector designed for use in resource-limited applications, Proc. Natl. Acad. Sci. U. S. A. 111 (2014) 11984–11989.
[11] K. Kerman, M. Saito, E. Tamiya, S. Yamamura, Y. Takamura, Nanomaterial-based electrochemical biosensors for medical applications, TrAC Trends Anal. Chem. 27 (2008) 585–592.
[12] Z. Dai, Z. Wang, Carbon nanomaterials-based electrochemical biosensors: an overview, Nanoscale 7 (2015) 6420–6431.
[13] D. Vilela, A. Martin, M.C. Gonzalez, A. Escarpa, Fast and reliable class-selective isoflavone index determination on carbon nanotube press-transferred electrodes using microfluidic chips, Analyst 139 (2014) 2342–2347.
[14] I. Švancara, K. Vytřas, K. Kalcher, A. Walcarius, J. Wang, Carbon paste electrodes in facts, numbers, and notes: a review on the occasion of the 50-years jubilee of carbon paste in electrochemistry and electroanalysis, Electroanalysis 21 (2009) 7–28.
[15] L. Tang, Y. Zhou, G. Zeng, Z. Li, Y. Liu, Y. Zhang, G. Chen, G. Yang, X. Lei, M. Wu, A tyrosinase biosensor based on ordered mesoporous carbon-Au/l-lysine/Au nanoparticles for simultaneous determination of hydroquinone and catechol, Analyst 138 (2013) 3552–3560.
[16] A. Martín, M.Á. López, M.C. González, A. Escarpa, Multidimensional carbon allotropes as electrochemical detectors in capillary and microchip electrophoresis, Electrophoresis 36 (2015) 179–194.
[17] Z. Zhu, L. Garcia-Gancedo, A.J. Flewitt, H. Xie, F. Moussy, W.I. Milne, A critical review of glucose biosensors based on carbon nanomaterials: carbon nanotubes and graphene, Sensors 12 (2012) 5996–6022.
[18] M. Valcárcel, S. Cárdenas, B.M. Simonet, Y. Moliner-Martínez, R. Lucena, Carbon nanostructures as sorbent materials in analytical processes, TrAC Trends Anal. Chem. 27 (2008) 34–43.
[19] T.M. Barnes, J. van de Lagemaat, D. Levi, G. Rumbles, T.J. Coutts, C.L. Weeks, D.A. Britz, I. Levitsky, J. Peltola, P. Glatkowski, Optical characterization of highly conductive single-wall carbon-nanotube transparent electrodes, Phys. Rev. B 75 (2007) (23541001–22354110).
[20] A. Merkoçi, M. Pumera, X. Llopis, B. Pérez, M. del Valle, S. Alegret, New materials for electrochemical sensing VI: carbon nanotubes, TrAC Trends Anal. Chem. 24 (2005) 826–838.
[21] A. Ambrosi, M. Pumera, Amorphous carbon impurities play an active role in redox processes of carbon nanotubes, J. Phys. Chem. C 115 (2011) 25281–25284.
[22] S.A. Bhakta, E. Evans, T.E. Benavidez, C.D. Garcia, Importance of protein adsorption onto nanomaterials for the development of biosensors and analytical devices, Anal. Chim. Acta 872 (2015) 7–25.
[23] E. Kibena, M. Marandi, V. Sammelselg, K. Tammeveski, B.B.E. Jensen, A.B. Mortensen, M. Lillethorup, M. Kongsfelt, S.U. Pedersen, K. Daasbjerg, Electrochemical behaviour of HOPG and CVD-grown graphene electrodes modified with thick anthraquinone films by diazonium reduction, Electroanalysis 26 (2014) 2619–2630.
[24] P. Fanjul-Bolado, P. Queipo, P.J. Lamas-Ardisana, A. Costa-García, Manufacture and evaluation of carbon nanotube modified screen-printed electrodes as electrochemical tools, Talanta 74 (2007) 427–433.
[25] P. Fanjul-Bolado, D. Hernández-Santos, P.J. Lamas-Ardisana, A. Martín-Pernía, A. Costa-García, Electrochemical characterization of screen-printed and conventional carbon paste electrodes, Electrochim. Acta 53 (2008) 3635–3642.
[26] C.D. Kuhnline, M.G. Gangel, M.K. Hulvey, R.S. Martin, Detecting thiols in a microchip device using micromolded carbon ink electrodes modified with cobalt phthalocyanine, Analyst 131 (2006) 202–207.
[27] Y. Ding, A. Ayon, C.D. Garcia, Electrochemical detection of phenolic compounds using cylindrical carbon-ink electrodes and microchip capillary electrophoresis, Anal. Chim. Acta 584 (2007) 244–251.
[28] Z. Nie, C.A. Nijhuis, J. Gong, X. Chen, A. Kumachev, A.W. Martinez, M. Narovlyansky, G.M. Whitesides, Electrochemical sensing in paper-based microfluidic devices, Lab Chip 10 (2010) 477–483.
[29] W. Dungchai, O. Chailapakul, C.S. Henry, Electrochemical detection for paper-based microfluidics, Anal. Chem. 81 (2009) 5821–5826.
[30] S. Donner, H.-W. Li, E.S. Yeung, M.D. Porter, Fabrication of optically transparent carbon electrodes by the pyrolysis of photoresist films: approach to single-molecule spectroelectrochemistry, Anal. Chem. 78 (2006) 2816–2822.
[31] Y. Dai, G.M. Swain, M.D. Porter, Zak Jerzy, New horizons in spectroelectrochemical measurements: optically transparent carbon electrodes, Anal. Chem. 80 (2008) 14–22.
[32] D. Sánchez-Molas, J. Cases-Utrera, P. Godignon, F. Javier del Campo, Mercury detection at microfabricated pyrolyzed photoresist film (PPF) disk electrodes, Sens. Actuator B-Chem. 186 (2013) 293–299.
[33] J. Kim, X. Song, K. Kinoshita, M. Madou, R. White, Electrochemical studies of carbon films from pyrolyzed photoresist, J. Electrochem. Soc. 145 (1998) 2314–2319.
[34] S. Ranganathan, R.L. McCreery, Electroanalytical performance of carbon films with near-atomic flatness, Anal. Chem. 73 (2001) 893–900.
[35] A. Mardegan, R. Kamath, S. Sharma, P. Scopece, P. Ugo, M. Madou, Optimization of carbon electrodes derived from epoxy-based photoresist, J. Electrochem. Soc. 160 (2013) B132–B137.
[36] K.C. Morton, C.A. Morris, M.A. Derylo, R. Thakar, L.A. Baker, Carbon electrode fabrication from pyrolyzed parylene C, Anal. Chem. 83 (2011) 5447–5452.
[37] S.A. Alharthi, T.E. Benavidez, C.D. Garcia, Ultra-thin optically transparent carbon electrodes produced from layers of adsorbed proteins, Langmuir 29 (2013) 3320–3327.
[38] G. Ruan, Z. Sun, Z. Peng, J.M. Tour, Growth of graphene from food, insects, and waste, ACS Nano 5 (2011) 7601–7607.
[39] W. Dungchai, O. Chailapakul, C.S. Henry, Use of multiple colorimetric indicators for paper-based microfluidic devices, Anal. Chim. Acta 674 (2010) 227–233.
[40] M.P. O'Halloran, M. Pravda, G.G. Guilbault, Prussian Blue bulk modified screen-printed electrodes for H_2O_2 detection and for biosensors, Talanta 55 (2001) 605–611.
[41] T.E. Benavidez, C.D. Garcia, Spectroscopic and electrochemical characterization of nanostructured optically transparent carbon electrodes, Electrophoresis 34 (2013) 1998–2006.
[42] E. Evans, E.F. Moreira, T.E. Benavidez, W.K.T. Coltro, C.D. Garcia, Modification of microfluidic paper-based devices with silica nanoparticles, Analyst 139 (2014) 5560–5567.
[43] E. Evans, E.F.M. Gabriel, W.K.T. Coltro, C.D. Garcia, Rational selection of substrates to improve color intensity and uniformity on microfluidic paper-based analytical devices, Analyst 139 (2014) 2127–2132.
[44] E.F.M. Gabriel, W.K.T. Coltro, C.D. Garcia, Fast and versatile fabrication of PMMA microchip electrophoretic devices by laser engraving, Electrophoresis 35 (2014) 2325–2332.
[45] L. Blanes, Maria F. Mora, Claudimir L. do Lago, A. Ayon, Carlos D. Garcia, Lab-on-a-chip biosensor for glucose based on a packed immobilized enzyme reactor, Electroanalysis 19 (2007) 2451–2456.
[46] M.R. Nejadnik, F.L. Deepak, C.D. Garcia, Adsorption of glucose oxidase to 3-D scaffolds of carbon nanotubes: analytical applications, Electroanalysis 23 (2011) 1462–1469.
[47] K. Scida, P.W. Stege, G. Haby, G.A. Messina, C.D. Garcia, Recent applications of carbon-based nanomaterials to analytical chemistry: a critical review, Anal. Chim. Acta 691 (2011) 6–17.
[48] V. Cozzani, L. Petarca, L. Tognotti, Devolatilization and pyrolysis of refuse derived fuels: characterization and kinetic modelling by a thermogravimetric and calorimetric approach, Fuel 74 (1995) 903–912.
[49] I. Milosavljevic, V. Oja, E.M. Suuberg, Thermal effects in cellulose pyrolysis: relationship to char formation processes, Ind. Eng. Chem. Res. 35 (1996) 653–662.
[50] H. Yang, R. Yan, H. Chen, D.H. Lee, C. Zheng, Characteristics of hemicellulose, cellulose and lignin pyrolysis, Fuel 86 (2007) 1781–1788.
[51] A. Broido, A simple, sensitive graphical method of treating thermogravimetric analysis data, J. Polymer Sci. 7 (1969) 1761–1773.
[52] M.V. Ramiah, Thermogravimetric and differential thermal analysis of cellulose, hemicellulose, and lignin, J. Appl. Polym. Sci. 14 (1970) 1323–1337.
[53] A.M. Youssef, S. Kamel, M. El-Sakhawy, M.A. El Samahy, Structural and electrical properties of paper–polyaniline composite, Carbohydr. Polym. 90 (2012) 1003–1007.
[54] E.K. Walker, D.A. Vanden Bout, K.J. Stevenson, Carbon optically transparent electrodes for electrogenerated chemiluminescence, Langmuir 28 (2012) 1604–1610.
[55] T. Jawhari, A. Roid, J. Casado, Raman spectroscopic characterization of some commercially available carbon black materials, Carbon 33 (1995) 1561–1565.
[56] A.C. Ferrari, J. Robertson, Resonant Raman spectroscopy of disordered, amorphous, and diamondlike carbon, Phys. Rev. B 64 (2001) 075414.
[57] Y. Ohzawa, M. Mitani, T. Suzuki, V. Gupta, T. Nakajima, Preparation of negative electrodes for lithium-ion rechargeable battery by pressure-pulsed chemical vapor infiltration of pyrolytic carbon into electro-conductive forms, J. Power Sources 122 (2003) 153–161.
[58] A.C. Ferrari, J. Robertson, Interpretation of Raman spectra of disordered and amorphous carbon, Phys. Rev. B 61 (2000) 14095–14107.
[59] C.D. García, P.I. Ortiz, Glassy carbon electrodes modified with different electropolymerized resol prepolymer mixtures for phenol and derivatives quantification, Anal. Sci. 15 (1999) 461–465.
[60] J.E. O'Reilly, Oxidation-reduction potential of the ferro-ferricyanide system in buffer solutions, Biochim. Biophys. Acta 292 (1973) 509–515.
[61] A.J. Bard, L.R. Faulkner, Electrochemical Methods: Fundamentals and Applications, Wiley, 2000.
[62] P.M. Diakowski, Y. Xiao, M.W.P. Petryk, H.-B. Kraatz, Impedance based detection of chemical warfare agent mimics using ferrocene-lysine modified carbon nanotubes, Anal. Chem. 82 (2010) 3191–3197.
[63] S. Basuray, S. Senapati, A. Aijian, A.R. Mahon, H.-C. Chang, Shear and AC field enhanced carbon nanotube impedance assay for rapid, Sensitive, and mismatch-discriminating DNA hybridization, ACS Nano 3 (2009) 1823–1830.
[64] M.F. Cabral, J.D. Barrios, É.M. Kataoka, S.A.S. Machado, E. Carrilho, C.D. Garcia, A.A. Ayon, Computational, electrochemical, and spectroscopic, studies of acetylcholinesterase covalently attached to carbon nanotubes, Colloids Surf. B: Biointerfaces 2013 (2013) 624–629.
[65] O.M.S. Filipe, C.M.A. Brett, Characterization of carbon film electrodes for electroanalysis by electrochemical impedance, Electroanalysis 16 (2004) 994–1001.
[66] T.E. Benavidez, C.D. Garcia, Potential-assisted adsorption of bovine serum albumin onto optically transparent carbon electrodes, Langmuir 29 (2013) 14154–14162.
[67] T.E. Benavidez, D. Torrente, M. Marucho, C.D. Garcia, Adsorption and catalytic activity of glucose oxidase accumulated on OTCE upon the application of external potential, J. Colloid Interface Sci. 435 (2014) 164–170.
[68] N. Chauhan, C.S. Pundir, An amperometric uric acid biosensor based on multiwalled carbon nanotube–gold nanoparticle composite, Anal. Biochem. 413 (2011) 97–103.
[69] P.-Y. Chen, R. Vittal, P.-C. Nien, G.-S. Liou, K.-C. Ho, A novel molecularly imprinted polymer thin film as biosensor for uric acid, Talanta 80 (2010) 1145–1151.